Girolline is a sequence-context specific modulator of eIF5A activity

Yongjun Dang
Fudan University https://orcid.org/0000-0001-7237-1132
Mayumi Arata
RIKEN
Yuichi Shichino
RIEKN Cluster for Pioneering Research https://orcid.org/0000-0002-0093-1185
Ali Al Mourabit
Institut de Chimie des Substances Naturelles du CNRS
Daniel Romo
Baylor University https://orcid.org/0000-0003-3805-092X
Jun Liu
Johns Hopkins University https://orcid.org/0000-0003-3842-9841
Shintaro Iwasaki
RIKEN https://orcid.org/0000-0001-7724-3754
Minoru Yoshida
RIKEN Center for Sustainable Resource Science https://orcid.org/0000-0002-4376-5674
Tilman Schneider-Poetsch (tsp@riken.jp)
RIKEN Center for Sustainable Resource Science

Article

Keywords: eIF5A, Girolline, Translation, Ribosome-associated quality control, Hypusination, Ribosome stalling, Mitochondria

Posted Date: June 15th, 2023

DOI: https://doi.org/10.21203/rs.3.rs-3027748/v1

Abstract

Natural products have a long history of providing potent probes into protein biosynthesis, with numerous molecules serving as valuable therapeutics. The marine natural product girolline has been described as an inhibitor of protein synthesis. Here, we demonstrate that it is not a general translation inhibitor but represents a sequence-specific modulator of translation factor eIF5A. Girolline interferes with ribosome-eIF5A interaction and induces ribosome stalling, primarily on AAA-encoded lysine. Our data furthermore indicate that eIF5A plays a physiological role in ribosome-associated quality control (RQC) and is important in maintaining the efficiency of translational progress. Girolline, therefore, provides a potent tool compound for understanding the interplay between protein production and quality control in a physiological setting and offers a new and selective means of modulating gene expression.

Introduction

Natural products have proven valuable tools in the elucidation of ribosome-catalyzed protein biosynthesis. Translation inhibitors have become potent therapeutics for the treatment of bacterial infections. The current pandemic highlights the need for specific medications in the fight against infectious diseases. This need is not limited to the treatment of viral or bacterial infections but extends to parasitic maladies. Girolline[1] (giro, also known as girodazole, Fig. 1A) was first isolated from *Pseudaxinyssa cantharella* marine sponge extracts and described as an anti-tumor agent as well as having activity against malaria[2–6].

Giro was characterized as a translation inhibitor several decades ago, with some suggestion of it inhibiting the termination process[5,7]. However, though its binding site on the large ribosomal subunit had been identified[8], neither mechanism of action nor therapeutic use has ever been thoroughly explored.

Recent developments in methodology have allowed describing the action of translation modulators not only in terms of their molecular mechanism but also in their cellular context, providing a comprehensive overview of changes to the entire proteome and translatome [9–11].

Previous mechanistic studies on translation modulators were often hampered by describing the molecule's activity in the isolation of an *in vitro* system, thereby failing to observe the compound's physiological effect. Especially sequence-specific modulation of translation often went undetected. Ribosome profiling[10,12] overcomes this issue and has brought to light context-dependent effects of translation inhibitors[11]. Context-dependent inhibition of translation provides an avenue to selectively target part of the proteome rather than inhibiting translation in a global manner.

Employing ribosome profiling and recently developed disome profiling[13–16], we revisited giro to explore its activity across the translatome. In this study, we could confirm that giro interferes with protein synthesis but did not find evidence for inhibition of translation termination[3]. Rather, giro acts in a sequence-dependent context and causes increased ribosomal stalling on amino acid sequences where translation

appears to slow down. It interferes with the ability of translation elongation factor eIF5A to interact with the ribosome.

eIF5A represents one of the most puzzling proteins regulating the synthesis of polypeptides. Originally identified as an initiation factor, it appears to play a far more important role in translation elongation[17–20]. So far, it is also the only protein known to carry a hypusine post-translational modification, derived from spermidine and attached to eIF5A lysine-50 in a two-step process by the dedicated enzymes dehydroxyhypusine synthetase (DHS) and dehydroxyhypusine hydroxylase (DOHH)[19,21–23]. While eIF5A is not required for translation *in vitro*, eIF5A constitutes an essential gene and loss of either eIF5A or DHS is lethal[17,24]. Defects in eIF5A or its hypusination are associated with various disease states, including neurodegeneration and cancer [25–28]. In particular, the decrease of hypusination in the aging process has been associated with mitochondrial degeneration[29,30]. eIF5A appears to aid the ribosome through structurally challenging amino acid stretches, such as poly-proline sequences[31,32]. Yet, the role of hypusine remains incompletely understood and specific chemical probes into eIF5A function are lacking, while indirect probes targeting the polyamine or hypusination machinery leave a lot to be desired.

Our data suggest that the role of eIF5A extends beyond helping the ribosome across poly-proline stretches. It appears eIF5A aids translational progress and prevents ribosomes from stalling, thereby preventing premature activation of the ribosome quality control pathway. Girolline modulates eIF5A behavior, causing increased ribosomal stalling on AAA-encoded lysine codons, especially when preceded by basic amino acid stretches.

Results

Ribosome stalling induced by giro

First, we set out to characterize giro's inhibitory activity on protein synthesis in mammalian cells. Through metabolic labeling of newly synthesized proteins with *O*-propargyl-puromycin (OP-puro) (Fig. 1B), an aminoacyl-tRNA mimic carrying a click-chemistry compatible alkyne which allows conjugation to a fluorescent dye, we did observe a decrease in protein synthesis by giro in a dose-dependent manner. However, we also noticed that giro did not inhibit translation to the same extent as a conventional translation elongation inhibitor such as cycloheximide (CHX). When looking at the distribution of ribosomal populations via sucrose density gradient centrifugation (Fig. 1C), we observed a decrease in the 80S population but an increase in the polysome fraction. We conducted the same experiment in an *in vitro* translation system using [^{32}P]-labeled rabbit β-globin mRNA. The data indicated an increase in the early polysome population (Fig. S1A). This increase in polysomes contradicts general translation initiation inhibition, which often results in polysome depletion. Rather, it is consistent with translation elongation inhibition, which stalls ribosomes in the middle of open reading frames (ORFs).

To get a global view of ribosome traversal along ORFs, we conducted monosome profiling, a deep sequencing based-method for ribosome footprints generated by RNase digestion[12], on giro-treated HEK293T cells. In view of potential ribosome stalling by the compound, we also employed disome profiling which sequences the mRNA fragments protected by two closely adjacent ribosomes, caused by slow elongation of the leading ribosome[13–16]. Both monosome and disome footprints were increased at the 5' end of the ORF (Fig. 1D), while the population around the stop codon was reduced (Fig. 1E). Especially the disome population decreased significantly towards the 3’ end. This suggested increased stalling towards the 5' end with fewer ribosomes reaching the stop codon. We noted that there was no indication of stop-codon read-through (Fig. 1E), which contradicts earlier reports of giro interfering with translation termination[4].

More quantitatively, we calculated the polarity score of footprint reads, a value indicating whether the average read distribution shifted towards the 5' end (negative) or the 3' end (positive)[32]. As expected, we saw a polarity score shift in direction toward the 5' end in both monosome and disome profiling (Fig. 1F and 1G). The change in ribosome distribution towards the 5’ end could also be observed when representing the data as a cumulative fraction plot (Fig. 1H), showing that giro treated samples generally had lower polarity scores than control. Together, these data indicate that giro does not completely block translational activity, though the observed decrease in protein output may stem from increased ribosomal stalling.

Sequence-selective stalling

In addition to the global effect of giro on elongation, we investigated whether ribosomal stalling occurred on a particular sequence element. Therefore, we focused on the disome profiling data and analyzed overrepresentation of individual amino acids in the ribosomal A, P, and E sites (Fig. 2A). In the ribosomal P site, Pro (P) and Phe (F) appeared to increase while Gln (Q), Glu (E), and especially Lys (K) were overrepresented in the E site. This overrepresentation was also observed in our monosome data (Fig. S2A). Motif analysis for disome enriched codons further narrowed down the sequence context for giro-mediated ribosome pausing. Both 1 and 10 µM giro led to similar sequence enrichment: Lys/Pro-Pro-Pro and Lys/Pro-Phe-Pro across E,P and A sites (Fig. 2B). We then considered dipeptide motifs occupying E and P-site or P and A-site. High disome occupancy in E and P-site containing di-amino acid pairs Lys-Pro and Lys-Phe further underlined the importance of these sequences for giro’s activity (Fig. 2C). In a similar manner, we observed a significant increase of di-amino acid motifs containing P-site proline when considering P and A-site occupancy under giro treatment, including Pro-Pro. Disome formation on an individual Lys-Pro site inside the COX6C gene exemplifies the context specificity of giro (Fig. 2D). The mapped monosome data along the COX6C ORF also shows a decrease of ribosome density towards the 3’ end.

Given the enrichment of Lys in the E site, we wondered whether giro would show preference for one of the two lysine codons (AAA or AAG) in inducing ribosomal stalling. Intriguingly, we found a more pronounced increase in E-site AAA than AAG for disome formation (Fig. 2E). Sequence enrichment analysis for E-site

AAA or AAG codons (Fig. S2B) led to the same conclusion. This was further highlighted by the disome occupancy of E and P-site with di-codon pairs, such as AAA-CCU (Lys-Pro), AAA-UUU (Lys-Phe), and AAA-CCG (Lys-Pro) (Fig. 2F). Moreover, unbiased motif analysis also showed enriched AAA, but not AAG, in the E site (Fig. S2C). These data demonstrated a unique context specificity for giro in inducing ribosomal stalling.

Displacement of eIF5A

We were furthermore intrigued by the increase in P and A-site proline. Increased stalling on poly-proline motifs is usually associated with insufficient levels of the translation factor eIF5A[16,31–33] (Fig. S2D, E). Giro's effect on translation looked like a combination of reduced eIF5A with additional stalling on E-site lysine. An involvement of eIF5A appeared possible, since the girolline binding site on the large ribosomal subunit of *Haloarcula marismortui* is known to lie in the vicinity of where eIF5A and the ribosome interact in eukaryotes (Fig. S3A)[8,34]. Furthermore, the binding site sits in an area of high sequence homology between archaea and eukaryotes (Fig. S3B) making binding in the same position on ribosomes of both phyla likely.

To determine whether giro binding affected the interaction between eIF5A and the ribosome, we used FLAG-tagged eIF5A for pulldown experiments. Tagged wild-type eIF5A did pull down ribosomes as shown by immunoblotting for small and large ribosomal subunit proteins, while the S51A mutant of eIF5A did not seem to interact with the ribosome (Fig. 3A, Fig. S3D). As most overexpressed eIF5A was reported to remain non-hypusinated[35], we co-expressed DHS and DOHH, which are responsible for the generation of dehydroxyhypusine and then hypusine on lysine 50[21,22], together with tagged eIF5A. Giro was able to interfere with the binding of hypusinated, and to a lesser extent also non-hypusinated eIF5A to the ribosome (Fig. 3A). It further blocked binding in a dose-dependent manner (Fig. 3B, S3E), when DOHH and DHS were co-expressed.

Thus far an involvement of eIF5A in the translation of the AAA codon has not been reported. We queried whether giro treatment induced ribosomal pausing in the same vicinity as pausing caused by eIF5A depletion (Fig. 3C). Focusing on significant pause sites detected under eIF5A depletion, we mapped pause sites induced by 10 µM giro treatment 30 nucleotides upstream and downstream of the giro-induced stall site. Both giro treatment and eIF5A depletion caused stalling on almost the same position, though with slight differences. eIF5A depletion showed a number smaller peaks 3' of the main pause site.

This corresponds to our observation on an individual gene level. When we compared disome footprint distribution between giro treated cells and cells with RNAi-depleted eIF5A, we found a number of transcripts, such as ATP5B, COX7A2, and NDUFC1 where giro application produced ribosomal stalling in the exact same location as eIF5A depletion (Fig. 3D). In a few other instances, giro caused stalling at different codons than the eIF5A-knockdown-induced stall sites (Fig. 3E). Such was the case for PPT1, HIST2H2AA3, and RPL38. As can be seen in the sequence of the individual stall sites, Giro did not always induce stalling on AAA-codons. Rather it seemed to prefer areas where some stalling seems to occur naturally, as seen by a small number of disome footprints present even in the absence of external

perturbation. It appears likely that translation slows in these areas, relying on eIF5A to maintain speed and fidelity.

AAA-specific stalling on reporter transcripts

To test whether we could replicate stalling on AAA-encoded lysine and test eIF5A involvement, we utilized fluorescent FACS reporter constructs, encoding enhanced green fluorescent protein (EGFP) and red fluorescent protein (RFP) connected by a short linker sequence [36]. Flanked by P2A sites[37], which allow the ribosome to proceed in-frame without amino-acid incorporation, the reporter produces three separate polypeptides from one transcript: EGFP as an internal control, the linker, and RFP as experimental readout (Fig. 4A)[36]. If translation stalls on the linker, less RFP is produced. Cells were transfected with vector constructs 48 h before cell sorting and treated with 1 µM giro for the last 16 h. We used empty linker $K(_0)$ for control and as expected did not see any effect of giro on either EGFP or RFP expression (Fig. 4B). Then we proceeded with a linker sequence containing twenty consecutive lysines encoded by $(AAA)_{20}$ or $(AAG)_{20}$ respectively (Fig. 4C, D). Twenty AAA codons in a row induced translational stalling with a modest reduction in RFP output compared to $K(_0)$ control, as reported previously[36]. However, giro treatment significantly reduced RFP production further (Fig. 4C). In many cases, RFP levels were reduced but not completely inhibited, visible in the FACS profile as the filling in of the “valley” between RFP negative cells and cells with high RFP expression (arrow). Giro affected only the expression of RFP when preceded by the $(AAA)_{20}$-linker, while it had no discernible effect on a linker containing 20 consecutive AAG codons (Fig. 4D). Furthermore, on a shorter version of the linker containing only 12 AAA codons, 1 µM giro had very little effect while stronger reduction of RFP production required a 5 µM dose (Fig. S4A). This corroborated our suspicion that giro requires a slowdown in translation to act and 20 AAA-encoded lysines seem to cause more slowing than 12. These data suggest that giro presents a sequence context-dependent translation modulator, which primarily causes ribosomal stalling on AAA-encoded lysine.

We then assessed eIF5A involvement, testing our FACS vectors in cells with RNAi-reduced levels of eIF5A. On cells transfected with non-targeting siRNA, giro showed the same reduction in RFP expression observed in non-transfected cells (Fig. 5A top). Even in the absence of giro, eIF5A knocked-down cells showed reduced RFP production on reporters containing the $(AAA)_{20}$-linker (Fig. 5A bottom). The FACS profiles of eIF5A-depleted cells are virtually indistinguishable from cells with normal levels of eIF5A after treatment with 1 µM giro (c.f. Figure 4C). Treating eIF5A knockdown cells with giro further reduced RFP expression, likely by preventing residual eIF5A from interacting with the ribosome (Fig. 5A bottom). eIF5A depletion only affected translation of the $(AAA)_{20}$-linker; using the $(AAG)_{20}$ construct, eIF5A depletion did not lead to detectable changes in RFP output (Fig. 5B).

Premature translation termination by RQC activation

The FACS reporters used in this study were originally designed for research on ribosome-associated quality control (RQC) and a recent study provided some evidence for eIF5A involvement in the RQC pathway[38]. RQC triggers when the cell detects collided ribosomes via the E3 ubiquitin ligase ZNF598 or

the ATPase ASCC3[39]. It involves separating the ribosomal subunits and destroying the nascent peptide by ubiquitination through the Ltn1 E3 ligase and the addition of non-templated alanine and threonine amino acids to the peptide's C-terminus by NEMF, known as CAT-tailing[40]. Translation of poly-A tails in mammalian cells constitutes an established way of inducing RQC.

This led us to investigate the effect of giro on RQC induction. We modified our FACS reporter (Fig. 4A) to monitor premature translation termination and ribosomal stalling (Fig. 6A). We deleted the N-terminal P2A site and added a stop codon to the end of the linker. This construct now produced EGFP with a C-terminal tail sequence, consisting of either 20 AAA codons or 20 GAA codons. If translation was to proceed unimpeded, we expected to see a full-length band of ~ 48 kDa. Stalling and premature termination would produce a shortened protein, detectable by immunoblotting against EGFP. As expected, control cells showed some level of stalling made worse by the addition of giro (Fig. 6B), indicated by an increase in the detectable proteins smaller than 48 kDa.

eIF5A knock-down itself (Fig. S5A) led to an increase of these shortened proteins similar to treatment with 1 µM giro. Therefore, eIF5A appeared to aid the translation of poly-A stretches. This would support our hypothesis that giro acts in areas of translational slowing and would suggest that eIF5A plays a role in maintaining speed and fidelity of translation elongation beyond poly-proline stretches.

When RQC triggers ASCC3 or ZNF598 are knocked down (Fig. S5A), giro loses its effect, and translation proceeds to full length (Fig. 6B). The translational complexes stalling on a poly-A sequence should still be translation-competent and probably proceed to the end of the reading frame by themselves if RQC does not engage. When RQC factors Ltn1 and NEMF were depleted, more stalling was observed possibly because depletion of these downstream protein degradation factors slows down clearing of stalled ribosomal complexes further (Fig. 6B). Importantly, prematurely terminated peptides were only observed on the $(AAA)_{20}$ construct, while the translation of $(GAA)_{20}$ did complete unimpeded, irrespective of giro treatment or RQC factor knockdown (Fig. 6C). Corroborating our FACS data, even 20 consecutive AAG codons did not cause visible stalling irrespective of giro treatment or eIF5A-knockdown (Fig S5B). It is known that the AAA codon presents more challenges to the translation machinery than AAG[41,42]. This appears due to adenosine nucleotides potentially forming single-stranded helices, interfering with decoding[43]. In addition, the positively charged lysine, especially in case of poly-lysine sequences, appears to force the peptidyl tRNA into an unfavorable conformation.

This underlines that eIF5A is only required when translation slows down but does not act as a general elongation factor.

Effects on gene expression

Since giro-induced stalling occurs in a cellular context, we were curious about which translational response giro would induce. Simultaneous RNA sequencing from the same material used in ribosome profiling allowed us to measure changes in translation efficiency (TE). We observed significantly altered TE at higher giro concentration. Few genes appeared affected at 1 µM (Fig. S6A) while 10 µM giro

produced a much stronger result. We observed increased expression of genes relating to protein synthesis, likely a result of the cell trying to compensate for decreased protein output (Fig. S6B and Supplementary Table 1)[44,45]. We also saw upregulation of adenosylmethionine decarboxylase (AMD1), a gene involved in polyamine synthesis[46]. Since the polyamine spermidine is a source for the hypusine modification on eIF5A[21], this regulation may be another means to counteract giro's function to inhibit eIF5A. At the same time, splicing factors and heat shock proteins appeared to decrease in expression (Fig. S6B and S6D). Stalling does not necessarily mean termination of translation and in a number of genes affected by giro we did not detect a significant reduction in protein levels (data not shown).

Mitochondrial phenotype

eIF5A also plays a role in mitochondrial maintenance[29,30] and reduced hypusination levels on eIF5A during the aging process have been associated with mitochondrial deterioration. We compared giro's impact on mitochondria to DHS inhibitor GC7, which significantly reduces eIF5A hypusination levels[47]. We tested whether giro would affect mitochondrial function by both fluorescent microscopy and metabolome analysis in comparison to GC7 treatment. Mitochondria were stained with MitoTracker Red and immunostained against the outer mitochondrial membrane protein TOMM20. Giro treatment displayed a modest effect on mitochondrial morphology with some thinning of the mitochondrial network (Fig. S7A). In contrast, treatment with 30 μM GC7 obliterated mitochondrial structure and led to a breakup of the mitochondrial network into small circular structures.

To further test whether giro inhibited mitochondrial translation, we used mitochondrial fluorescent non-canonical amino acid tagging (mito-FUNCAT) for metabolic labeling[48]. We detected a slight decrease in mitochondrial protein synthesis when treating cells with 1 and 5 μM giro overnight, while GC7 significantly inhibited mitochondrial translation (Fig. S7B). In terms of TCA intermediates, we did observe a reduction in α-ketoglutarate, malate, and fumarate, but did not see a reduction in citrate or isocitrate by giro treatment (Fig. S7C). In contrast, 30 μM GC7 treatment led to marked depletion of either metabolite (Fig. S7D).

Although our findings confirmed that giro treatment also impacts mitochondrial physiology, GC7 appeared to have a stronger effect than giro. 1 μM giro or 30 μM GC7 correspond to the IC_{50} for inhibition of cell proliferation. While GC7 treatment does decrease overall protein synthesis[27], we could neither detect a change in ribosomal stalling behavior nor in the polarity of ribosome distribution (data not shown). We suspect that part of GC7's impact on mitochondria may result from activity unrelated to eIF5A hypusination (Matsumoto et al. manuscript in preparation).

Discussion

In summary, we demonstrate that giro constitutes a sequence context-specific modulator of eIF5A function. Giro decreases eIF5A binding to the ribosome and increases ribosomal stalling, preferentially on AAA-encoded lysine at the E-site where eIF5A locates. We demonstrated that lack of eIF5A also causes

ribosomal stalling on poly-A sequences, hinting at a yet overlooked role of this translation factor. Perhaps, eIF5A not only prevents ribosomal stalling on poly-proline sequences as previously reported[31,32] but is also involved in maintaining translational fidelity in a wider range of challenging mRNA sequence contexts.

In particular, we have seen increased giro-induced stalling when E-site AAA-encoded lysine was preceded by P-site proline. Perhaps, the combination of E-site lysine and P-site proline with giro is mechanistically similar to E-site proline and P-site proline without eIF5A. In both cases stalling on P-site proline occurs in combination with an E-site amino acid that has already undergone two rounds of peptidyl transfer. Structural studies will shine more light on the molecular details of giro's sequence context-specifc mechanism of protein synthesis inhibition.

Knockdown of ASCC3 and ZNF598 overcame ribosomal stalling on poly-A sequences, underlining that reduced protein output and premature termination on the $(AAA)_{20}$-sequence were due to RQC involvement. A recent structural study identified eIF5A as part of RQC complexes and suggested that it plays a role in peptide formation during CAT-tailing[40]. It is important to consider that this involvement of eIF5A takes place after the ribosomal subunits have been split apart. While we would support the notion that eIF5A plays a role in RQC, our data suggest that, while translation is in progress, eIF5A prevents RQC activation.

We propose a kinetic model (Fig. 7) in which translation proceeds without eIF5A involvement, as long as the translated message does not contain challenging sequence stretches (Fig. 7A). When the translation is impeded by difficult-to-translate sequences, including poly-proline, but also AAA-encoded lysine, eIF5A helps to maintain translational progression (Fig. 7B). If eIF5A function is altered, either by reduced protein levels or by giro preventing eIF5A from interacting with the ribosome, increased stalling occurs, triggering RQC activation (Fig. 7C). Thereby, eIF5A maintains translational fidelity and prevents premature RQC processing.

When RQC triggering is hampered by depletion of ZNF598 or ASCC3 giro loses its ability to cause stalling on poly-A stretches. Since the complexes stalled on poly-A remain elongation-competent, preventing RQC activation appears to allow translation to proceed to completion. In other contexts, where stalled ribosomes are incapable of continuing elongation, we would expect a lack of RQC trigger factors to increase stalling and decrease protein output. The lack of giro-induced translational inhibition of the $(GAA)_{20}$ and $(AAG)_{20}$ reporters or of EGFP itself underlines that girolline does not act as a general translation inhibitor but requires the right sequence context to show an effect. Likely a slowing of translational progress makes the ribosome accessible for giro binding. We suspect that a number of conditions coincide when ribosomes stall either through giro treatment or through lack of sufficient eIF5A. These conditions likely include stretches of positively charged amino acids interacting with the rRNA around the nascent peptide tunnel, as well as a slowing of decoding on A-rich mRNA sequences[41]. We calculated the average isoelectric point (pI) for the amino acids in the nascent peptides of our disome fraction as a measure for positive charge. We noticed an increase in average pI about 4 to 7 amino acids

upstream from the A-site (Fig S8A). This effect was even more pronounced when only considering the giro-stalled disome fractions containing AAA in the E-site (Fig S8B). We noticed for several transcripts, such as HIST2H2AA3, COX7A or SNRPC, that the increase in detected disome footprints coincided with areas of positively charged amino acids (Fig S8C). This would further support the idea that charge-charge interactions between nascent peptide and rRNA in the nascent peptide tunnel provide part of the physiological context for giro to have an effect.

Furthermore, the conformation of E-site lysine and P-site proline amino acids under giro treatment will contribute to the observed sequence-specific stalling phenotype. Since stalling occurs preferentially, but not exclusively on AAA-encoded lysine or poly-proline stretches under either giro treatment or eIF5A depletion, this combination of conditions most likely determines location and strength of the induced ribosomal pause site.

In terms of a wider physiological context, the observed involvement of eIF5A in aging and the maintenance of mitochondrial health[49,50] may not be the result of one particular protein not being properly expressed, but rather a “death by a thousand cuts”, with decreasing translational fidelity leading to increased stalling, premature processing by the RQC machinery and a slowly deteriorating proteome.

As giro acts directly on the ribosome and rather than indirectly altering eIF5A behavior through inhibition of hypusination, we expect it to become a useful tool compound for triggering RQC and for globally modulating eIF5A function in various physiological settings. Given the difficulty in genetically manipulating eIF5A due to the lethality, we think giro will be of particular interest in the study of eIF5A involvement in aging and neurodegeneration.

Despite its known effect on cancer cell proliferation, giro’s therapeutic potential has not been comprehensively explored. It did enter clinical trials against neoplasms in the past, though they seem not to have advanced past phase I, owing to dose-limiting toxicity and no observed anti-tumor effect[51]. Perhaps more intriguing is the reported anti-malarial activity. *Plasmodium falciparum* mRNAs are AT rich and carry poly-A stretches in their coding regions[52]. Our findings finally provide a mechanistic explanation for girolline’s toxicity against *Plasmodium*. Given the enormous societal toll malaria still exacts, girolline should be re-evaluated for its potential in anti-parasitic therapy. It is possible that sequence-context specific inhibition of protein synthesis could provide sufficient selectivity to offer a therapeutic window for giro to be explored as a novel antimalarial agent. We are therefore confident that giro will prove a useful chemical probe for research on translation, aging, and mitochondrial health and beyond.

Significance

We present the first sequence-context-specific modulator of eIF5A activity, which prevents the interaction between its target protein and the large ribosomal subunit and induces ribosomal stalling, especially on AAA-encoded lysine. We demonstrate that eIF5A ensures speedy translation and plays a role in preventing the premature degradation of nascent peptides by the ribosome-associated quality control pathway. In

addition, we demonstrate that giro treatment also exerts a physiological effect on mitochondria. We further think that giro has great potential as a chemical probe to understand the role of eIF5A in a wide variety of physiological contexts and may provide a basis for the development of further sequence-selective translational modulators.

Materials and Methods

Tissue culture

HEK293 Flp-In T-Rex cells (Thermo Fisher Scientific, R78007), HEK293T cells and HeLa S3 cells (gift from Prof. Fumio Hanaoka, University of Tokyo) were grown at 37°C and 5% CO_2 in DMEM high glucose medium with glutamine (Wako), supplemented with antibiotics and 10% fetal bovine serum.

Compounds

GC7 powder was dissolved in 10 mM acetic acid to a final concentration of 30 mM and stored at − 30°C. Girolline (synthesized by Dr. Ali Al Mourabit and provided by Dr. Daniel Romo) was dissolved in DMSO to 100 mM stock concentration and stored at − 30°C.

FLAG-tag pulldowns

The ORFs of human eIF5A, DOHH and DHS were amplified from reverse-transcribed Hela cell mRNA and cloned into pcDNA3.1 vectors with N-terminal Flag or V5 tags.

Flag-tagged wildtype eIF5A or the eIF5A S51A mutant were overexpressed in HEK293T cells with or without V5-tagged DHS and DOHH. After 24 hours, cells were treated with 10 µM giro for 1 hour and lyzed in TMK100 buffer (20 mM Tris-HCl pH 7.4, 100 mM KCl, 5 mM $MgCl_2$, 2 mM DTT, 1% Triton-X 100, 100 U/ml RNasIN in DEPC RNase free water). Identical amounts of lysate were incubated with Flag M2 antibody-conjugated agarose beads (Sigma) for 1 h. After 3 washes with TMK100 buffer, beads were boiled in 1x SDS loading buffer and separated by SDS-PAGE for Western blotting and silver staining.

RNAi

Cells were plated in 6-well format at 500.000 cells per well overnight, treated with 90 pmol RNAi constructs (Dharmacon ON-TARGETplus siRNAs) against eIF5A1 (L-015739-00-0005), ASCC3 (L-012757-01-0005), ZNF598 (L-007104-00-0005), LTN1 (L-006968-00-0005), NEMF (L-019106-02-0005), or non-targeting control (D-001810-10-05) using Thermo Lipofectamine RNAiMax according to the manufacturer's instructions, and incubated for 72 h before analysis. Knock-down was confirmed by Western blot.

FACS analysis

Cells seeded in 6-well plates were transfected with 2 µg plasmid DNA [either pmGFP-P2A-K0-P2A-RFP (Addgene plasmid # 105686; http://n2t.net/addgene:105686; RRID:Addgene_105686), pmGFP-P2A-

K(AAA)12-P2A-RFP (Addgene plasmid # 105687; http://n2t.net/addgene:105687; RRID:Addgene_105687), pmGFP-P2A-K(AAA)20-P2A-RFP (Addgene plasmid # 105688; http://n2t.net/addgene:105688; RRID:Addgene_105688), or pmGFP-P2A-K(AAG)20-P2A-RFP (Addgene plasmid # 105688; http://n2t.net/addgene:105688; RRID:Addgene_105688); gifts from Ramanujan Hegde] and 8 µl X-tremeGENE HP (Roche), incubated for 24 h, and then treated with compounds at the indicated concentrations for 14 h. Cells were washed once with cold PBS, trypsinized, and quenched with PBS containing 10% fetal bovine serum. Cell suspensions were then pipetted into 5-ml round bottom polystyrene tubes with a cell strainer (Falcon, cat# 352235) and kept on ice until analysis on a FACSAria II Special Order System (BD).

DNA construction

pmGFP-P2A-K(AAA)20-P2A-RFP was modified for use in Western Blotting [53]. The vector was digested with SalI and KpnI before custom synthesized DNA inserts were created, deleting the N-terminal P2A site and adding a stop codon before the C-terminal P2A sequence. These inserts either kept the $(AAA)_{20}$ sequence or changed it to $(GAA)_{20}$. Vector maps and sequences were provided in Supplementary Vector Map.

Polysome profiling

Polysome profiling was carried out as before [54,55]. Briefly, HEK293T cells were grown to close to confluency in 15-cm dishes. 50 µM giro or DMSO solvent control was applied for 60 min. Cells were briefly washed in cold PBS and lysed in 30 mM Tris-HCl pH 7.4, 100 mM KCl, 5 mM $MgCl_2$, 2 mM DTT, and 1% Triton-X 100. Lysates were cleared by centrifugation at 20,000 × g at 4°C for 10 min. Aliquots containing the same amount of RNA normalized by OD_{254} were loaded onto 15–45% sucrose gradients and centrifuged for 90 min at 40,000 rpm in an SW41Ti swing bucket rotor (Beckman Coulter). The distribution of ribosomes was monitored by OD_{254} through an in-line spectrophotometer.

For *in vitro* polysome profiles, β-globin mRNA was reverse transcribed with T7 RNA polymerase in the presence of 1 mM ATP, CTP, UTP, and 0.5 mM GTP as well as 30 µCi α-[^{32}P] GTP and 2 mM m^7G cap analog using a commercial kit (Ribomax, Promega). An aliquot of 200 ng of radiolabeled RNA was added to 25 µl rabbit reticulocyte (RRL) translation reactions supplemented with KCl, DTT, and amino acids, as described above. After incubation at 30°C for 15 min, samples were diluted to a total volume of 200 µl in gradient buffer (20 mM Hepes-KOH pH 7.4, 100 mM KCl, 5 mM $MgCl_2$, and 2 mM DTT) and centrifuged through 15-35% sucrose gradients using an SW55Ti rotor (Beckman Coulter) at 50,000 rpm at 4°C. Two hundred microliter fractions were collected by hand and scintillation-counted on a Perkin Elmer Microbeta luminometer.

Labeling of newly synthesized proteins with OP-puro

The procedure was carried out as in Chhipi-Shrestha et al. [56]. Briefly, 250,000 HEK293T cells/well were plated into 24-well plates and grown overnight. The next day, the medium was replaced with 500 µl fresh

culture medium containing girolline at the indicated concentrations in triplicate. As a control 100 µg/ml of cycloheximide (CHX) was included. Cells were incubated for 90 min before the dropwise addition of 50 µl Opti-MEM containing 200 µM *O*-propagyl-puromycin (Jena Bioscience). Cells were incubated for a further 30 min before washing with 500 µl ice-cold PBS. After careful removal of the medium, cells were collected in cold 60 µl lysis buffer (20 mM Tris-HCl pH 7.5, 150 mM NaCl, 5 mM $MgCl_2$, and 1% Triton-X 100) by pipetting up and down followed by 10 min incubation on ice. The lysate was cleared by centrifugation at 20,000 × *g* for 10 min at 4°C. Fifteen micro litter lysate was reacted with 0.4 µl of 50 µM IRdye800CW (LI-COR Biosciences) using a Click-it cell reaction kit (Thermo Fisher Scientific) according to the manufacturer's instructions and incubated at 25°C for 30 min. Meanwhile, G-25 gel filtration columns (Cytiva) were washed thrice with 500 µl lysis buffer containing 1 mM DTT by centrifugation at 740 × *g* for 1 min at 4°C.

The click reaction was then loaded onto the washed columns and spun at 740 × *g* for 2 min at 4°C. The eluted lysate was mixed with 6 µl 6× IR-compatible loading buffer (LI-COR Biosciences) and heated to 95°C for 5 min. Ten micro litter aliquots were loaded onto a 5–20% gradient gel and resolved at a constant 20 mA current in 1× SDS buffer. The gel was then briefly washed in MilliQ water and fixed with a 50% methanol and 7% acetic acid solution for 15 min. The gel was washed for 15 min in MilliQ water before visualizing on an Odyssey CLx (LI-COR Biosciences) at the 800-nm channel and quantitation of the signal per lane. Afterward, the gel was stained with Coomassie by incubation with Gel Code Blue reagent (Thermo Fisher Scientific) for 30 min and then washed in MilliQ water overnight. The gel was again scanned on the Odyssey CLx scanner and the total protein was quantified using the 700-nm channel. Data was analyzed by dividing the IR800 signal by the Coomassie signal at IR700.

Mito-FUNCAT

Metabolic labeling of mitochondrial translation was performed as in Kimura et al. [41]. A day before the experiment HEK293 Flp-In T-Rex cells were plated out at 250,000 cells per well in 1 ml medium into 12-well plates in triplicate for each condition. Cells were then incubated with compounds at the indicated concentration overnight before the culture medium was replaced with methionine-free DMEM containing 50 µM HPG and 1 µg/ml anisomycin to block cytosolic translation. The labeling medium also contained giro, GC7, or solvent control DMSO at the indicated concentration. After 3 h incubation, the cells were collected by pipetting up and down, spun down at 3000 × *g* for 3 min at 4°C and washed once with ice-cold PBS. The supernatant was carefully removed and the cell pellet was lysed in 35 µl lysis buffer (20 mM Tris-HCl pH 7.5, 150 mM NaCl, 5 mM $MgCl_2$, and 1% Triton-X 100) by pipetting up and down and incubating on ice for 10 min. Debris was pelleted by centrifugation at 20,000 × *g* for 10 min at 4°C. Thirty micro litter supernatant was reacted with 50 µM IRdye800CW (LI-COR Biosciences) in 40 µl total volume for 30 min, using a Click-it cell reaction kit (Thermo Fisher Scientific) according to the manufacturer's instructions. The reacted lysate was spun through G-25 gel filtration (Cytiva) columns at 740 × *g* for 2 min at 4°C and heated in 17 µl of 6× IR-compatible loading buffer (LI-COR Biosciences) at 50°C for 5 min. Fifteen micro litter lysate was then run on a 5–20% gradient Bolt gel (Thermo Fisher Scientific) in 1× MES running buffer (Thermo Fisher Scientific). The gel was then fixed in 50% methanol and 7% acetic acid for

15 min before washing with MilliQ water for 3 h. Infrared (IR) signal at 800 nm was then measured on an Odyssey CLx (LI-COR Biosciences) before staining the gel with GelCode™ Blue reagent (Thermo) overnight. The next day total protein was quantified again by an Odyssey CLx (LI-COR Biosciences) at 700-nm channel.

Fluorescent microscopy

HeLa S3 cells were plated on glass coverslips at 50,000 cell per well in 24-well formats and incubated overnight in 1 ml of tissue culture medium. The next day, Mitotracker Red CMXRos was added to 250 nM final concentration for 45 min. Cells were washed once with PBS at 37°C and then fixed with 4% paraformaldehyde in PBS for 15 to 20 min at 37°C. The cover slips were washed three times in PBS containing 0.2% Triton-X 100 (PBS-Tri), before blocking for 1 h in 1% BSA dissolved in PBS-Tri. Primary antibody for mitochondrial outer membrane marker TOMM20 (SCBT, sc-17764, 1:40) was added at 1:50 dilution in 1% BSA/PBS-Tri solution and incubated overnight at 4°C. After three more washes, Alexa Fluor 488-conjugated secondary antibody was added to 1:1000 in 1% BSA/PBS-Tri and incubated at room temperature for 1 h. Cells were washed thrice more by PBS-Tri, with the first wash containing DAPI stain at 0.1 µg/ml. The cover slips were then mounted on glass slides with Diamond antifade mounting agent and allowed to be set overnight. Cells were visualized on a Deltavision fluorescent microscope (Image Solutions).

Metabolome analysis

Detection of TCA metabolites was based on Al Kadhi et al. [57]. HEK293 Flp-In T-Rex cells were plated out at 1 million cells/well in 6-well formats and in quadruplicate on the day before the experiment and treated with 30 µM GC7, 1 µM or 5 µM giro, or solvent control DMSO overnight. One well was used for cell counting before the remaining three wells were processed by aspirating the culture medium and quickly washing each well with 1 ml ice-cold 0.9% NaCl solution. After carefully removing the wash, cells were lysed with 640 µl ice-cold methanol and 320 µl MilliQ water and 100 nM d4-deuterated succinate as internal control. Lysates were collected and cleared by centrifugation at 19,000 × *g* for 10 min at 4°C. The supernatant was collected and dried down under a vacuum at 30°C and then processed for mass spectrometry .

Monosome profiling, disome profiling, and RNA-Seq

Lysate preparation

Library preparation was conducted as previously reported [16,58]. HEK293 Flp-In T-Rex cells were plated to 1 × 10^7 cells in 10-cm dishes. Cells were treated for 2 h with either DMSO solvent control or 1, and 10 µM giro. For eIF5A knock-down samples, cells were transfected with Dharmacon smartPool siRNA (L-015739-00-0005) 72 h before lysis, as described earlier [16]. Cells were washed once with ice-cold PBS and then lysed in 600 µl lysis buffer (20 mM Tris-HCl pH 7.5, 150 mM NaCl, 5 mM $MgCl_2$, 1% Triton-X 100, 1 mM DTT, 100 µg/ml cycloheximide, and 100 µg/ml chloramphenicol). Lysates were digested with DNase and

cleared by centrifugation. After determining RNA concentration by Qubit BR (Thermo Fisher Scientific), lysate containing 10 µg of RNA was used for each sample.

Library preparation, monosome and disome profiling

Libraries were prepared as previously reported [58]. The lysate containing 10 µg RNA was scaled up to 300 µl by lysis buffer, and digested with 2 µl (10 U/µl) RNase I (Epicentre) for 45 min at 25°C. The reaction was stopped by the addition of SUPERase•IN RNase inhibitor (Thermo Fisher Scientific) and cooling samples on ice. The digested RNA solution was then placed on a 900 µl 1 M sucrose cushion and centrifuged for 1 h at 100,000 rpm, 4°C in a TLA110 ultracentrifuge rotor (Beckman Coulter). The pellet was dissolved in 300 µl TRIzol reagent (Thermo Fisher Scientific) and RNA was purified using the Direct-zol RNA MicroPrep Kit (Zymo Research) according to the manufacturer's instructions. The purified RNA was then separated by gel electrophoresis. For monosome analysis a gel slice ranging from 17–34 nt was excised and for disomes from 50–80 nt. Fragments were purified, ligated into sequencing adapters, and rRNA-depleted using the Ribo-Zero kit gold kit, included in the TruSeq Stranded total RNA-sequencing kits (Illumina). After PCR amplification, disome libraries were cleaved with a custom gRNA and Cas9 protein as described earlier [58].

Library preparation, RNA-Seq

For TE analysis, RNA from 50 µl aliquots of the lysates were purified with the Direct-zol Micro kit (Zymo research) and 1 µg total purified RNA was then depleted of rRNA and cloned into sequencing adapter using the Illumina TruSeq Stranded Total RNA Library Prep Gold kit according to the manufacturer's instructions. Libraries were sequenced on an Illumina HiSeq4000 sequencer, using single ended 50 bp reads for monosome profiling and 150 bp for disome profiling and RNA-sequencing.

Data analysis

Data analysis was conducted as published previously [16,59,60]. Monosome and disome occupancies were calculated as the ratio of reads at a given codon to the average reads per codon on that transcript. Disome pause sites were defined as codons with disome occupancies larger than the mean plus 1 standard deviation. Translational efficiency was calculated with DESeq2[61]. The first and last 5 codons of each CDS were omitted from the analysis. Monosonome and disome profiling data with eIF5A knockdown and the control were obtained from our previous study GSE145723[16].

Ontology analysis was performed using DESEQ2 [61] expression analysis combined withclusterProfiler [62] and EnhancedVolcano (https://github.com/kevinblighe/EnhancedVolcano) for gene set analysis.

Motifs associated with ribosome stalling were illustrated with kpLogo[63]. Data obtained from DMSO solvent control or non-targeting siRNA pool was used for background deduction.

pI was calculated within a 6 amino acid window of the nascent chain of the stalled ribosome using the R Peptides package.

Overlaps in the pause site were calculated by taking average disome reads from eIF5A-depleted cells that not only lay one standard deviation above the mean but also where the ratio of normalized reads in experiment over control was > 1.5. Disome reads from 10 μM giro-treated samples were then mapped within 30 nucleotides upstream and downstream of the eIf5A-kd pause site.

All custom scripts used in this study are available upon request.

Western blot

Cell Lysates were collected in 1x SDS Buffer (50 mM Tris-HCl pH 6.8, 2% SDS, 10% glycerol, 1% β-mercaptoethanol, 12.5 mM EDTA, 0.02% bromophenol blue) and denatured by heating to 95°C for 10 min. Five to fifteen micro litter aliquots were run on 5–20% gradient gels in Laemmli buffer and then transferred onto nitrocellulose membranes (BioRad). Membranes were blocked with Intercept TBS blocking buffer (LI-COR Biosciences) for 1 h and incubated overnight with primary antibodies in Intercept TBS blocking buffer. Unless otherwise noted, antibody dilution was 1:1000. Antibodies used in this study were as follows: anti-tubulin (1:5000; SCBT, sc-23948), anti-eIF5A (BD Biosciences, 611977), anti-ZNF598 (Thermo Fisher Scientific, PA5-31410), anti-NEMF (Thermo Fisher Scientific, PA5-49768), anti-LTN1 (1:500; Thermo Fisher Scientific, PA5-42315), anti-ASCC3 (Proteintech, 17627-1-AP), anti-GFP (Abcam, ab290), anti-RPS6 (Cell Signal, S2217), anti-RPL36a (SCBT, sc100831), anti-RPL3 (SCBT, sc86826) and anti-FLAG M2 (Sigma, F1804). After incubation, membranes were washed thrice in TBS-T (0.5% Tween) buffer for 15 min before incubation with a secondary antibody (anti-mouse antibody conjugated with IRDye 680CW, LI-COR Biosciences, 926-68070 or anti-rabbit antibody conjugated with IRDye 800RD, LI-COR Biosciences, 926-68071) for 1 h at 1:10,000 dilution.

Accession numbers

Mosome profiling, disome profiling, and RNA-Seq data obtained in this study are available in the GEO depository under accession number: GSE233886.

Declarations

Acknowledgments

We thank members of the Yoshida and Iwasaki labs for constructive discussions and technical help, especially Mari Mito for providing helpful technical advice on ribosome profiling, as well as Hironori Saito and Peixun Han for help with data processing. Ken Matsumoto and Rumi Kurokawa provided helpful insights on GC7 and its effect on mitochondria, as well as constructive comments on experimental data. We are indebted to Kenji Ohtawa and Masaya Usui of the RIKEN Center for Brain Science for FACS and metabolite GC/MS analysis.

Funding

T.S.P. was supported by a RIKEN Shorei Incentive Grant. M.Y. was supported in part by a Grant-in-Aid for Scientific Research (S) (JP19H05640) from the Japan Society for the Promotion of Science (JSPS) and a

Grant-in-Aid for Scientific Research on Innovative Areas (JP18H05503) from the Ministry of Education, Culture, Sports, Science and Technology (MEXT).

S.I. was supported by the Japan Agency for Medical Research and Development (AMED) (AMED-CREST, JP23gm1410001), the Japan Society for the Promotion of Science (JSPS) [a Grant-in-Aid for Scientific Research (B), JP23H02415], the Ministry of Education, Culture, Sports, Science and Technology (MEXT) [a Grant-in-Aid for Transformative Research Areas (B) “Parametric Translation”, JP20H05784], and RIKEN (Pioneering Projects “Biology of Intracellular Environments”). Y.S. was supported by JSPS [a Grant-in-Aid for Scientific Research (C), JP23K05648] and MEXT [a Grant-in-Aid for Transformative Research Areas (A) “Multifaceted Proteins”, JP21H05734, JP23H04268].

Author contributions

Conceptualization and Methodology, T.S.P and Y.D.; Software, S.I., Y.S. and T.S.P.; Investigation, T.S.P, Y.D. and M.A. Resources, S.I., A.A.M. and D.R.; Writing - Original Draft, T.S.P; Review and Editing, T.S.P., K.M., S.I., Y.D. and M.Y. Project Administration and Supervision, M.Y., J.O.L, S.I.; Funding Acquisition, M.Y., S.I. and T.S.P.

Conflict of interest

The authors declare no conflict of interest.

References

1. Marchais, S., Al Mourabit, A., Ahond, A., Poupat, C. & Potier, P. A short synthesis of the marine bioactive metabolite (+/-) girolline. *Tetrahedron Lett* **39**, 8085-8088 (1998). https://doi.org:Doi 10.1016/S0040-4039(98)01814-0
2. Ahond, A. *et al.* Girolline, a New Antitumoral Compound Extracted from the Sponge, Pseudaxinyssa-Cantharella N-Sp (Axinellidae). *Cr Acad Sci Ii* **307**, 145-148 (1988).
3. Lavelle, F., Zerial, A., Fizames, C., Rabault, B. & Curaudeau, A. Antitumor activity and mechanism of action of the marine compound girodazole. *Invest New Drugs* **9**, 233-244 (1991). https://doi.org:10.1007/BF00176976
4. Colson, G., Rabault, B., Lavelle, F. & Zerial, A. Mode of action of the antitumor compound girodazole (RP 49532A, NSC 627434). *Biochem Pharmacol* **43**, 1717-1723 (1992). https://doi.org:10.1016/0006-2952(92)90701-j
5. Tsukamoto, S. *et al.* Girolline, an antitumor compound isolated from a sponge, induces G2/M cell cycle arrest and accumulation of polyubiquitinated p53. *Biol Pharm Bull* **27**, 699-701 (2004). https://doi.org:10.1248/bpb.27.699
6. Benoit-Vical, F., Salery, M., Soh, P. N., Ahond, A. & Poupat, C. Girolline: a potential lead structure for antiplasmodial drug research. *Planta Med* **74**, 438-444 (2008). https://doi.org:10.1055/s-2008-1034348

7. Fung, S. Y. *et al.* Unbiased screening of marine sponge extracts for anti-inflammatory agents combined with chemical genomics identifies girolline as an inhibitor of protein synthesis. *ACS Chem Biol* **9**, 247-257 (2014). https://doi.org:10.1021/cb400740c
8. Schroeder, S. J., Blaha, G., Tirado-Rives, J., Steitz, T. A. & Moore, P. B. The structures of antibiotics bound to the E site region of the 50 S ribosomal subunit of Haloarcula marismortui: 13-deoxytedanolide and girodazole. *J Mol Biol* **367**, 1471-1479 (2007). https://doi.org:S0022-2836(07)00159-3 [pii] 10.1016/j.jmb.2007.01.081
9. Ingolia, N. T. Ribosome profiling: new views of translation, from single codons to genome scale. *Nat Rev Genet* **15**, 205-213 (2014). https://doi.org:nrg3645 [pii] 10.1038/nrg3645
10. Iwasaki, S. & Ingolia, N. T. The Growing Toolbox for Protein Synthesis Studies. *Trends Biochem Sci* **42**, 612-624 (2017). https://doi.org:S0968-0004(17)30092-0 [pii] 10.1016/j.tibs.2017.05.004
11. Shichino, Y. & Iwasaki, S. Compounds for selective translational inhibition. *Curr Opin Chem Biol* **69** (2022). https://doi.org:ARTN 102158 10.1016/j.cbpa.2022.102158
12. Ingolia, N. T., Ghaemmaghami, S., Newman, J. R. & Weissman, J. S. Genome-wide analysis in vivo of translation with nucleotide resolution using ribosome profiling. *Science* **324**, 218-223 (2009). https://doi.org:10.1126/science.1168978
13. Arpat, A. B. *et al.* Transcriptome-wide sites of collided ribosomes reveal principles of translational pausing. *Genome Res* **30**, 985-999 (2020). https://doi.org:10.1101/gr.257741.119
14. Meydan, S. & Guydosh, N. R. Disome and Trisome Profiling Reveal Genome-wide Targets of Ribosome Quality Control. *Mol Cell* **79**, 588-602 e586 (2020). https://doi.org:10.1016/j.molcel.2020.06.010
15. Zhao, T. *et al.* Disome-seq reveals widespread ribosome collisions that promote cotranslational protein folding. *Genome Biol* **22**, 16 (2021). https://doi.org:10.1186/s13059-020-02256-0
16. Han, P. *et al.* Genome-wide Survey of Ribosome Collision. *Cell Rep* **31**, 107610 (2020). https://doi.org:10.1016/j.celrep.2020.107610
17. Schnier, J., Schwelberger, H. G., Smit-McBride, Z., Kang, H. A. & Hershey, J. W. Translation initiation factor 5A and its hypusine modification are essential for cell viability in the yeast Saccharomyces cerevisiae. *Mol Cell Biol* **11**, 3105-3114 (1991). https://doi.org:10.1128/mcb.11.6.3105-3114.1991
18. Kang, H. A., Schwelberger, H. G. & Hershey, J. W. The two genes encoding protein synthesis initiation factor eIF-5A in Saccharomyces cerevisiae are members of a duplicated gene cluster. *Mol Gen Genet* **233**, 487-490 (1992). https://doi.org:10.1007/BF00265449
19. Kang, H. A., Schwelberger, H. G. & Hershey, J. W. Translation initiation factor eIF-5A, the hypusine-containing protein, is phosphorylated on serine in Saccharomyces cerevisiae. *J Biol Chem* **268**, 14750-14756 (1993).
20. Schwelberger, H. G., Kang, H. A. & Hershey, J. W. Translation initiation factor eIF-5A expressed from either of two yeast genes or from human cDNA. Functional identity under aerobic and anaerobic conditions. *J Biol Chem* **268**, 14018-14025 (1993).

21. Park, M. H., Cooper, H. L. & Folk, J. E. Identification of hypusine, an unusual amino acid, in a protein from human lymphocytes and of spermidine as its biosynthetic precursor. *Proc Natl Acad Sci U S A* **78**, 2869-2873 (1981). https://doi.org:10.1073/pnas.78.5.2869
22. Abbruzzese, A., Park, M. H. & Folk, J. E. Deoxyhypusine hydroxylase from rat testis. Partial purification and characterization. *J Biol Chem* **261**, 3085-3089 (1986).
23. Cano, V. S. *et al.* Mutational analyses of human eIF5A-1–identification of amino acid residues critical for eIF5A activity and hypusine modification. *FEBS J* **275**, 44-58 (2008). https://doi.org:10.1111/j.1742-4658.2007.06172.x
24. Nishimura, K., Lee, S. B., Park, J. H. & Park, M. H. Essential role of eIF5A-1 and deoxyhypusine synthase in mouse embryonic development. *Amino Acids* **42**, 703-710 (2012). https://doi.org:10.1007/s00726-011-0986-z
25. Wu, G. Q., Xu, Y. M. & Lau, A. T. Y. Recent insights into eukaryotic translation initiation factors 5A1 and 5A2 and their roles in human health and disease. *Cancer Cell Int* **20**, 142 (2020). https://doi.org:10.1186/s12935-020-01226-7
26. Wang, Z., Jiang, J., Qin, T., Xiao, Y. & Han, L. EIF5A regulates proliferation and chemoresistance in pancreatic cancer through the sHH signalling pathway. *J Cell Mol Med* **23**, 2678-2688 (2019). https://doi.org:10.1111/jcmm.14167
27. Landau, G., Bercovich, Z., Park, M. H. & Kahana, C. The role of polyamines in supporting growth of mammalian cells is mediated through their requirement for translation initiation and elongation. *J Biol Chem* **285**, 12474-12481 (2010). https://doi.org:10.1074/jbc.M110.106419
28. Mathews, M. B. & Hershey, J. W. The translation factor eIF5A and human cancer. *Biochim Biophys Acta* **1849**, 836-844 (2015). https://doi.org:S1874-9399(15)00100-5 [pii] 10.1016/j.bbagrm.2015.05.002
29. Liang, Y. *et al.* eIF5A hypusination, boosted by dietary spermidine, protects from premature brain aging and mitochondrial dysfunction. *Cell Rep* **35**, 108941 (2021). https://doi.org:10.1016/j.celrep.2021.108941
30. Puleston, D. J. *et al.* Polyamines and eIF5A Hypusination Modulate Mitochondrial Respiration and Macrophage Activation. *Cell Metab* **30**, 352-363 e358 (2019). https://doi.org:10.1016/j.cmet.2019.05.003
31. Saini, P., Eyler, D. E., Green, R. & Dever, T. E. Hypusine-containing protein eIF5A promotes translation elongation. *Nature* **459**, 118-121 (2009). https://doi.org:10.1038/nature08034
32. Schuller, A. P., Wu, C. C., Dever, T. E., Buskirk, A. R. & Green, R. eIF5A Functions Globally in Translation Elongation and Termination. *Mol Cell* **66**, 194-205 e195 (2017). https://doi.org:S1097-2765(17)30170-3 [pii] 10.1016/j.molcel.2017.03.003
33. Gutierrez, E. *et al.* eIF5A promotes translation of polyproline motifs. *Mol Cell* **51**, 35-45 (2013). https://doi.org:10.1016/j.molcel.2013.04.021
34. Melnikov, S. *et al.* Crystal Structure of Hypusine-Containing Translation Factor eIF5A Bound to a Rotated Eukaryotic Ribosome. *J Mol Biol* **428**, 3570-3576 (2016).

https://doi.org:10.1016/j.jmb.2016.05.011

35. Lee, J. W., Bae, S. H., Jeong, J. W., Kim, S. H. & Kim, K. W. Hypoxia-inducible factor (HIF-1)alpha: its protein stability and biological functions. *Exp Mol Med* **36**, 1-12 (2004). https://doi.org:200402291 [pii] 10.1038/emm.2004.1
36. Juszkiewicz, S. *et al.* ZNF598 Is a Quality Control Sensor of Collided Ribosomes. *Mol Cell* **72**, 469-481 e467 (2018). https://doi.org:10.1016/j.molcel.2018.08.037
37. Kim, J. H. *et al.* High cleavage efficiency of a 2A peptide derived from porcine teschovirus-1 in human cell lines, zebrafish and mice. *PLoS One* **6**, e18556 (2011). https://doi.org:10.1371/journal.pone.0018556
38. Tesina, P. *et al.* Molecular basis of eIF5A-dependent CAT tailing in eukaryotic ribosome-associated quality control. *Mol Cell* **83**, 607-621 e604 (2023). https://doi.org:10.1016/j.molcel.2023.01.020
39. Hashimoto, S., Sugiyama, T., Yamazaki, R., Nobuta, R. & Inada, T. Identification of a novel trigger complex that facilitates ribosome-associated quality control in mammalian cells. *Sci Rep* **10**, 3422 (2020). https://doi.org:10.1038/s41598-020-60241-w
40. Kostova, K. K. *et al.* CAT-tailing as a fail-safe mechanism for efficient degradation of stalled nascent polypeptides. *Science* **357**, 414-417 (2017). https://doi.org:10.1126/science.aam7787
41. Koutmou, K. S. *et al.* Ribosomes slide on lysine-encoding homopolymeric A stretches. *Elife* **4** (2015). https://doi.org:10.7554/eLife.05534
42. Tesina, P. *et al.* Molecular mechanism of translational stalling by inhibitory codon combinations and poly(A) tracts. *EMBO J* **39**, e103365 (2020). https://doi.org:10.15252/embj.2019103365
43. Chandrasekaran, V. *et al.* Mechanism of ribosome stalling during translation of a poly(A) tail. *Nat Struct Mol Biol* **26**, 1132-1140 (2019). https://doi.org:10.1038/s41594-019-0331-x
44. Zencir, S., Dilg, D., Rueda, M. P., Shore, D. & Albert, B. Mechanisms coordinating ribosomal protein gene transcription in response to stress. *Nucleic Acids Res* **48**, 11408-11420 (2020). https://doi.org:10.1093/nar/gkaa852
45. Albert, B. *et al.* A ribosome assembly stress response regulates transcription to maintain proteome homeostasis. *Elife* **8** (2019). https://doi.org:10.7554/eLife.45002
46. Pegg, A. E. Functions of Polyamines in Mammals. *J Biol Chem* **291**, 14904-14912 (2016). https://doi.org:10.1074/jbc.R116.731661
47. Jakus, J., Wolff, E. C., Park, M. H. & Folk, J. E. Features of the spermidine-binding site of deoxyhypusine synthase as derived from inhibition studies. Effective inhibition by bis- and mono-guanylated diamines and polyamines. *J Biol Chem* **268**, 13151-13159 (1993).
48. Kimura, Y. *et al.* Mito-FUNCAT-FACS reveals cellular heterogeneity in mitochondrial translation. *RNA* **28**, 895-904 (2022). https://doi.org:10.1261/rna.079097.122
49. Stein, K. C., Morales-Polanco, F., van der Lienden, J., Rainbolt, T. K. & Frydman, J. Ageing exacerbates ribosome pausing to disrupt cotranslational proteostasis. *Nature* **601**, 637-642 (2022). https://doi.org:10.1038/s41586-021-04295-4

50. Schroeder, S. *et al.* Dietary spermidine improves cognitive function. *Cell Rep* **35**, 108985 (2021). https://doi.org:10.1016/j.celrep.2021.108985
51. Singh, R., Sharma, M., Joshi, P. & Rawat, D. S. Clinical status of anti-cancer agents derived from marine sources. *Anticancer Agents Med Chem* **8**, 603-617 (2008).
52. Pavlovic Djuranovic, S. *et al.* Plasmodium falciparum translational machinery condones polyadenosine repeats. *Elife* **9** (2020). https://doi.org:10.7554/eLife.57799
53. Juszkiewicz, S. & Hegde, R. S. Initiation of Quality Control during Poly(A) Translation Requires Site-Specific Ribosome Ubiquitination. *Mol Cell* **65**, 743-750 e744 (2017). https://doi.org:10.1016/j.molcel.2016.11.039
54. Schneider-Poetsch, T. *et al.* Inhibition of eukaryotic translation elongation by cycloheximide and lactimidomycin. *Nat Chem Biol* **6**, 209-217 (2010). https://doi.org:nchembio.304 [pii] 10.1038/nchembio.304
55. Dang, Y. *et al.* Inhibition of eukaryotic translation elongation by the antitumor natural product Mycalamide B. *RNA* **17**, 1578-1588 (2011). https://doi.org:rna.2624511 [pii] 10.1261/rna.2624511
56. Chhipi-Shrestha, J. K. *et al.* Splicing modulators elicit global translational repression by condensate-prone proteins translated from introns. *Cell Chem Biol* **29**, 259-275 e210 (2022). https://doi.org:10.1016/j.chembiol.2021.07.015
57. Al Kadhi, O., Melchini, A., Mithen, R. & Saha, S. Development of a LC-MS/MS Method for the Simultaneous Detection of Tricarboxylic Acid Cycle Intermediates in a Range of Biological Matrices. *J Anal Methods Chem* **2017**, 5391832 (2017). https://doi.org:10.1155/2017/5391832
58. Mito, M., Mishima, Y. & Iwasaki, S. Protocol for Disome Profiling to Survey Ribosome Collision in Humans and Zebrafish. *STAR Protoc* **1**, 100168 (2020). https://doi.org:10.1016/j.xpro.2020.100168
59. Ingolia, N. T., Brar, G. A., Rouskin, S., McGeachy, A. M. & Weissman, J. S. The ribosome profiling strategy for monitoring translation in vivo by deep sequencing of ribosome-protected mRNA fragments. *Nat Protoc* **7**, 1534-1550 (2012). https://doi.org:10.1038/nprot.2012.086
60. Iwasaki, S., Floor, S. N. & Ingolia, N. T. Rocaglates convert DEAD-box protein eIF4A into a sequence-selective translational repressor. *Nature* **534**, 558-561 (2016). https://doi.org:nature17978 [pii] 10.1038/nature17978
61. Love, M. I., Huber, W. & Anders, S. Moderated estimation of fold change and dispersion for RNA-seq data with DESeq2. *Genome Biol* **15**, 550 (2014). https://doi.org:10.1186/s13059-014-0550-8
62. Wu, T. *et al.* clusterProfiler 4.0: A universal enrichment tool for interpreting omics data. *Innovation (Camb)* **2**, 100141 (2021). https://doi.org:10.1016/j.xinn.2021.100141
63. Wu, X. & Bartel, D. P. kpLogo: positional k-mer analysis reveals hidden specificity in biological sequences. *Nucleic Acids Res* **45**, W534-W538 (2017). https://doi.org:10.1093/nar/gkx323

Figures

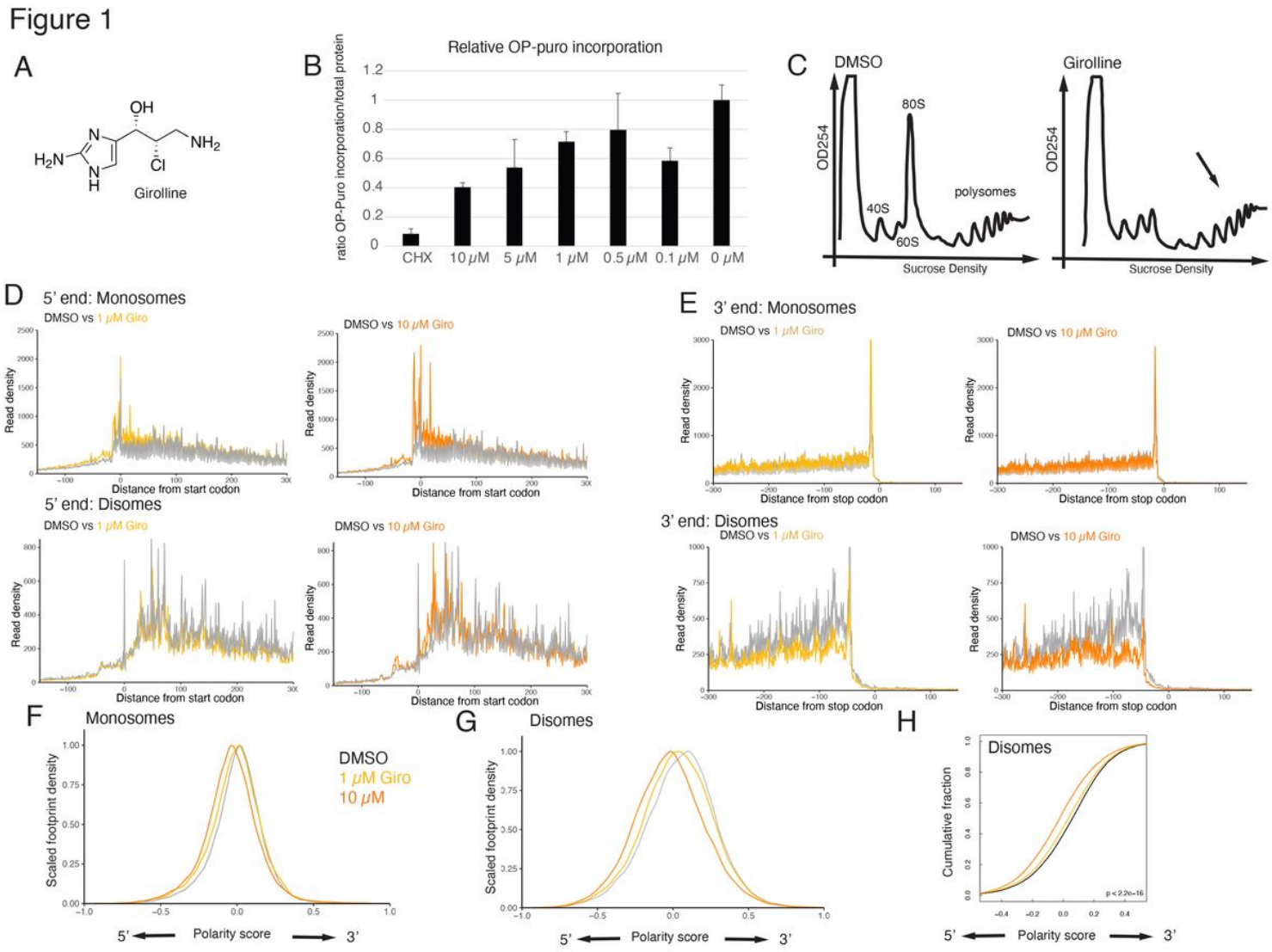

Figure 1

Girolline stalls translation

A. Structure of girolline. B. Reduction of protein synthesis over measured by metabolic labeling with OP-puro. The experiment was conducted in triplicate with background signal deduction and error bars denoting standard deviation. C. Polysome profiling from cells treated with DMSO control and 10 μM girolline. 80S ribosome populations appear decreased while polysomes increase (arrow). D. Metagene analysis of averaged ribosomal reads around the translation start site. Overlay of DMSO control (grey) and 1 μM giro (yellow) or 10 μM giro (orange) Reads were normalized by total read count and mapped -150 to 300 nucleotides from the start codon for both monosome and disome fractions. Disome read density appears increased towards the 5' end at increasing concentrations of giro. E. Metagene analysis of monosome and disome fractions -300 to 150 nucleotides from stop codon. Disome read density appears decreased with increasing giro concentration. F. Monosome polarity shift. Distribution of ribosome density across all open reading frames was evaluated. At increasing giro concentrations ribosome density shifted towards the 5'-end. G. This trend appeared more pronounced when evaluating

disome reads. H. Cumulative fraction plot of disome polarity data. Cumulative polarity score shifts toward 5’ end under giro treatment.

Figure 2

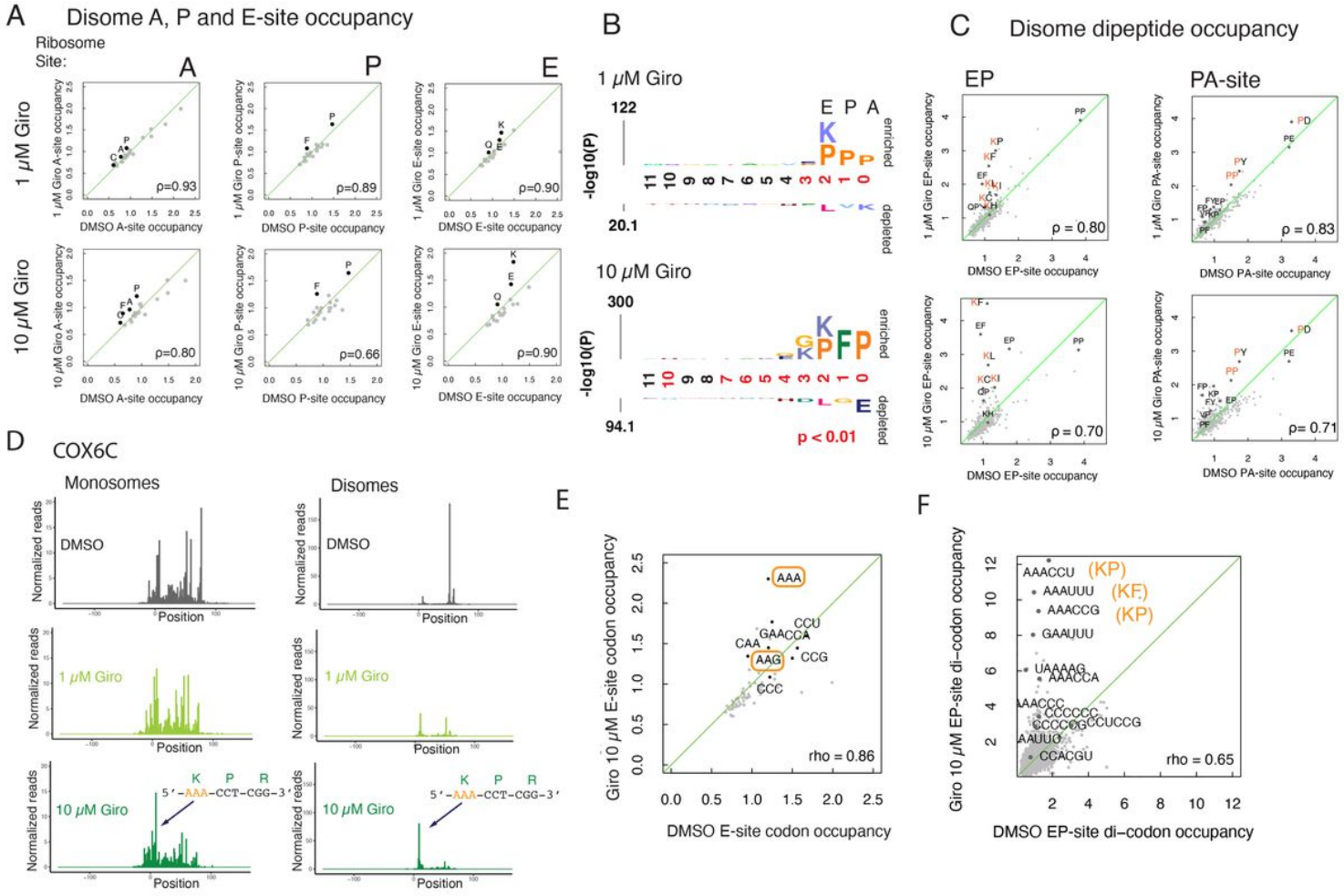

Figure 2

Sequence-specific stalling

A. Evaluation of increased A, P or E-site occupancy of disome fractions treated with 1 and 10 µM giro by graphing relative frequency of each amino acid per site under giro treatment against DMSO control. Dots above the green line denote overrepresented amino acids. We noticed a particular increase of proline and phenylalanine in the P-site and lysine in the E-site. B. Amino acid enrichment analysis using the kp-logo webtool, which also factors in a wider sequence context. Letters above the line denote the most significantly enriched amino acid in each position. Red numbers indicate a calculated p-value under 0.01 C. Further enrichment analysis, looking at dipeptides spanning E and P-site, as well as P and A-site. The combination of E-site lysine with P-site proline or phenylalanine appears especially frequent. In P and A-site, combinations with proline are enriched, including Pro-Pro. Enriched E-site lysine and P-site proline highlighted in orange. D. Ribosomal footprints from monosome and disome fractions mapped on the COX6C open reading frame. The main stalling site occurred on AAA-encoded lysine (sequence excerpt

magnified with position of A, P and E site indicated). E. Codon-wise enrichment analysis of 10 μM giroline treated cells on the E-site. Even though less frequent in the genome than AAG, the AAA codon for lysine appeared more strongly enriched (orange outlines). F. Codon-wise enrichment analysis for E and P-site. AAAUUU coding for lysine and phenylalanine, as well as AAA-CCU and AAA-CCG both encoding lysine and proline were enriched (orange captions).

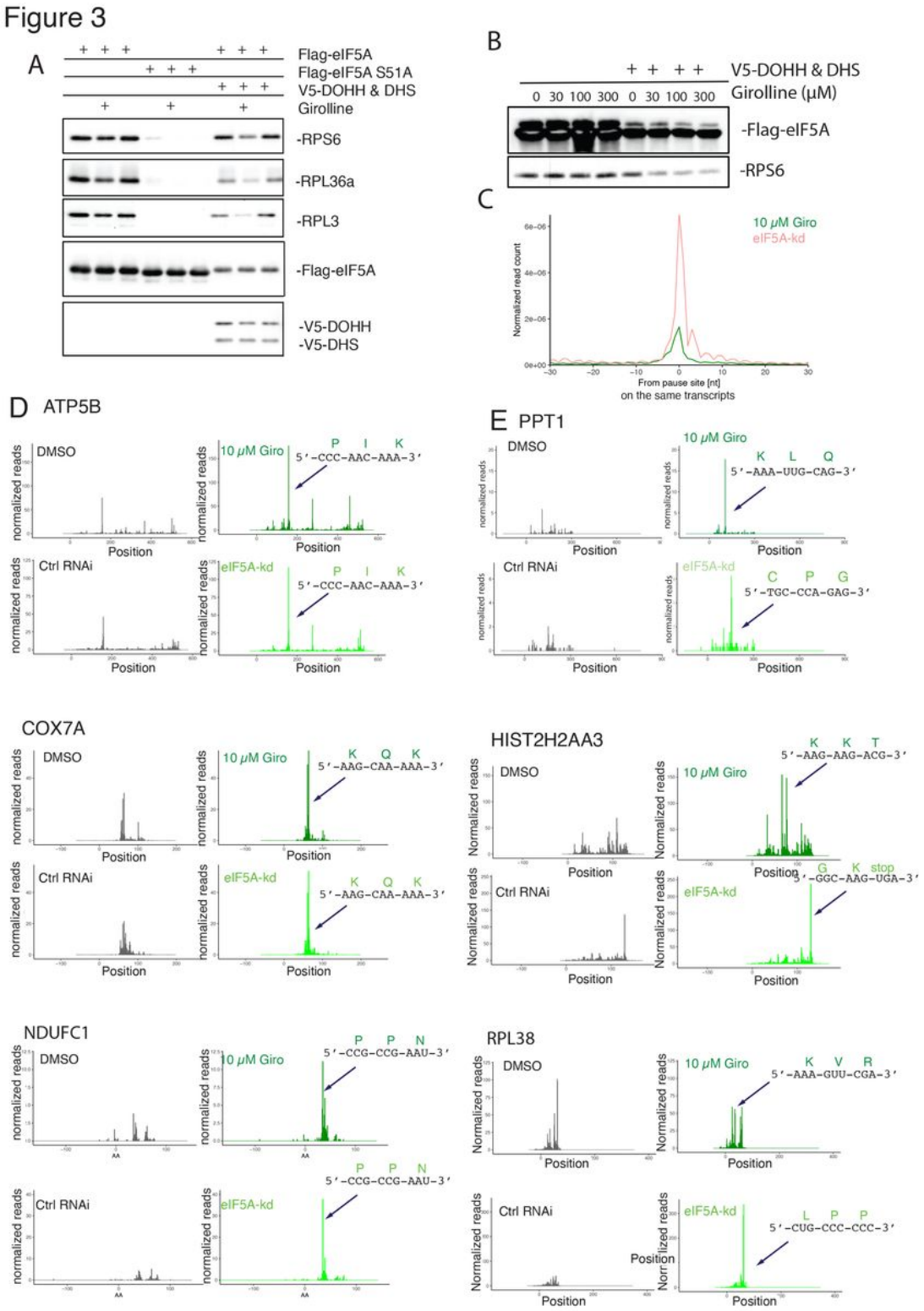

Figure 3

Girolline interferes with ribosome-eIF5A interaction

A. Girolline interferes with the binding of hypusinated eIF5A to the ribosome. Flag-tagged eIF5A was used for affinity pulldown of the ribosome. When hypusinating enzymes DOHH and DHS were overexpressed to ensure eIF5A hypusination the amount of pulled down ribosome decreased in the presence of girolline. B. Girolline displaced eIF5A from the ribosome in a dose-dependent manner. C. Metagene analysis of significant pause sites. Genes with significant eIF5A knockdown-induced pause sites (1 standard deviation above the mean for reads in each gene and at least 1.5 fold more average reads in eIF5A-knockdon than control RNAi) were probed for location of pause sites under 10 μM giro. Stalling appeared to largely occur in the same position, though eIF5A depletion showed a number of smaller peaks 3` of the main pause site. Peak sizes are not quantitative as two independent experiments are compared for position of the pause site. Ribosomal signals were normalized by the number of total disome reads per sample. D. Disome footprints mapped across the coding regions of ATP5B, COX7A and NDUFC1. The footprint distribution induced by 10 μM girolline was virtually indistinguishable from that caused by RNAi depletion of eIF5A. The coding sequence of the stall site with corresponding amino acids for A, P and E site are indicated, showing that girolline-induced stalling could also occur on sequences other than AAA. E. Disome footprints mapped across the coding region of PPT1 HIST2H2AA3 (HIST2AC18) and RPL38. In these cases giro-induced ribosomal stalling occurred just 5’ of the stall site induced by lack of eIF5A, in case of PPT1 and RPL38 the stall site did include E-site AAA.

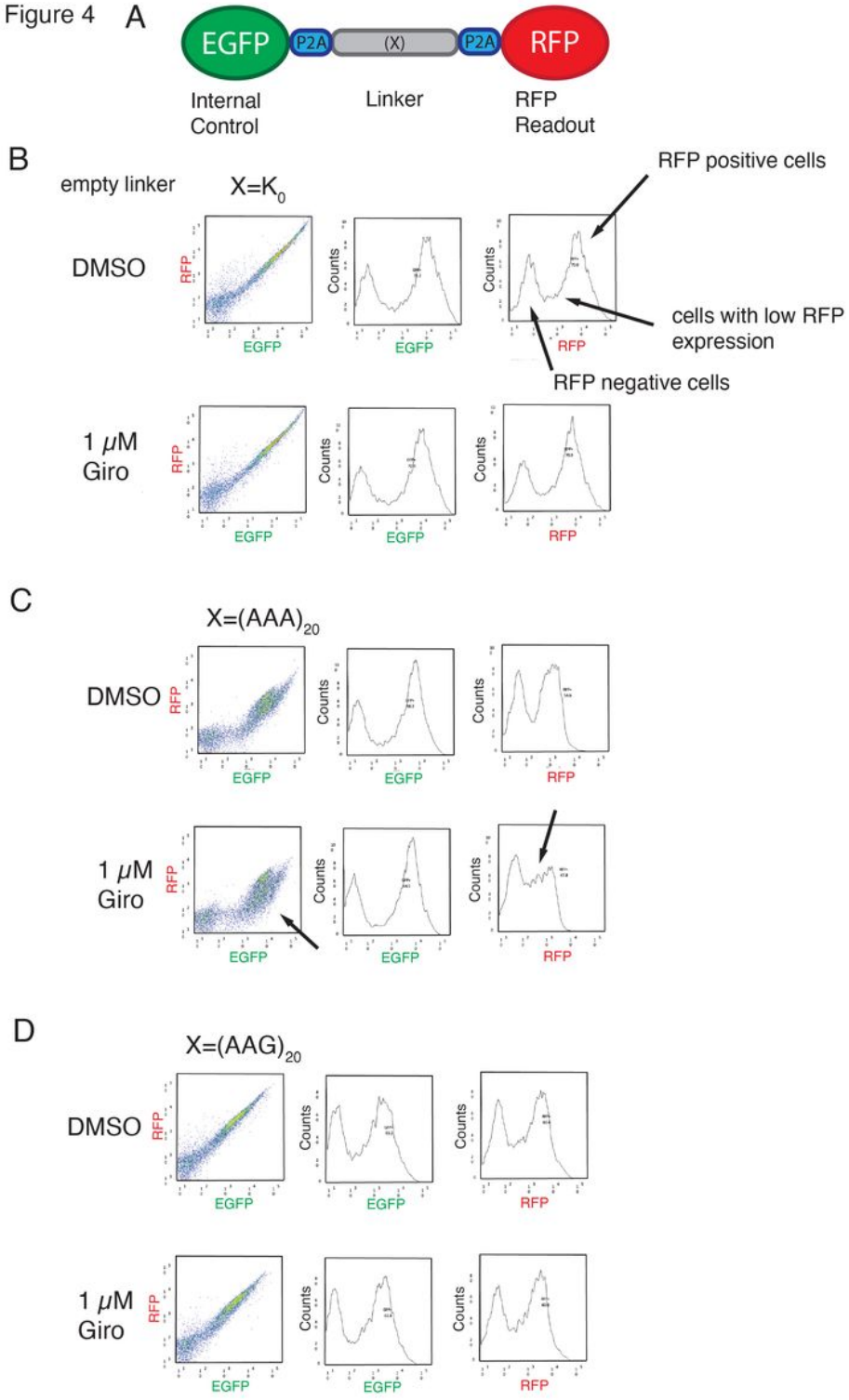

Figure 4

Sequence-specific stalling on FACS-reporters

A. FACS reporter used in this study. The vector will produce three peptides from one transcript: EGFP, linker and RFP. The linker sequence was varied for each set of experiments.
B. Control readout for empty linker. If translation of EGFP and RFP proceeds unperturbed the EGFP vs

RFP plot will show a straight line. The EGFP and RFP histograms show two peaks for non-fluorescing cells (left) and fluorophore positive cells (right) with a clear “valley” in between (see arrows). 1 µM girolline did not affect expression of either EGFP or RFP when using empty linker and yielded the same profile as DMSO treated cells. C. 1 µM giro reduced expression of RFP when the linker contained 20 consecutive AAA lysine codons. The RFP vs EGFP plot shows cells with high EGFP but low RFP expression (arrow in left panel). The “valley” is filled in with cells only expressing low amounts of RFP (arrow in right panel). D. This reduction in RFP expression was not observed when using a linker with 20 consecutive AAG lysine codons instead.

Figure 5

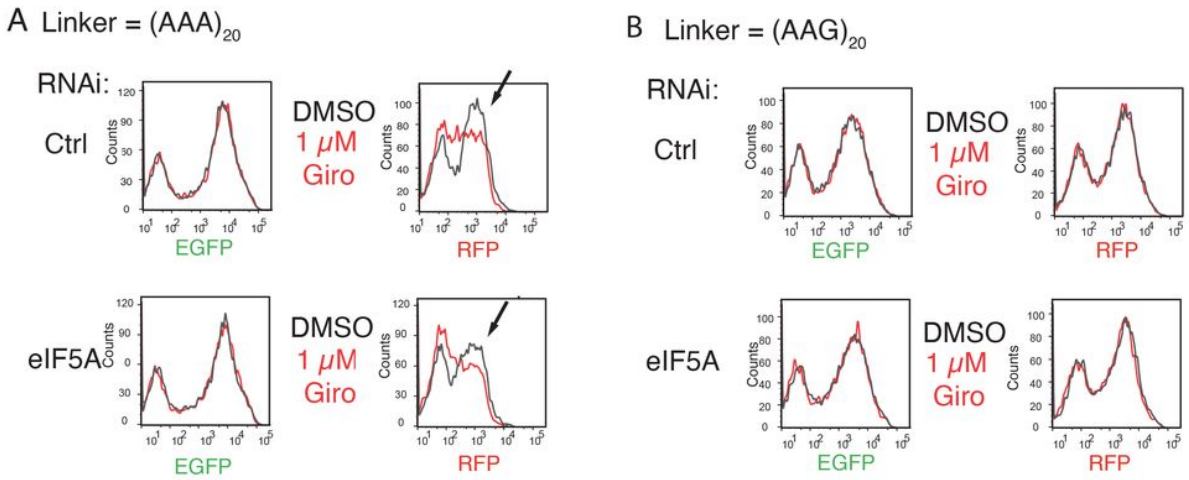

Figure 5

eIF5A is required for unimpeded AAA translation

Overlay of EGFP and RFP expression for non-targeting pool (top) and eIF5A-kd (bottom) treated with 1 µM giro (red). A. eIF5A is also required for translating the linker with 20 consecutive AAA lysine codons. A. top: 1 µM giro has the same effect on cells transfected with non-targetting RNAi pool as on non-transfected cells (cf. Fig 4B). A. bottom: eIF5A knockdown has a similar phenotype to giro treatment on control cells. RFP production is markedly decreased (cf. height of arrows). Adding 1 µM giro to eIF5A-kd cells decreases RFP expression further, likely by interfering with residual eIF5A. B. Neither eIF5A depletion nor giro treatment have an effect on a FACS construct containing a linker of 20 consecutive AAG codons.

Figure 6

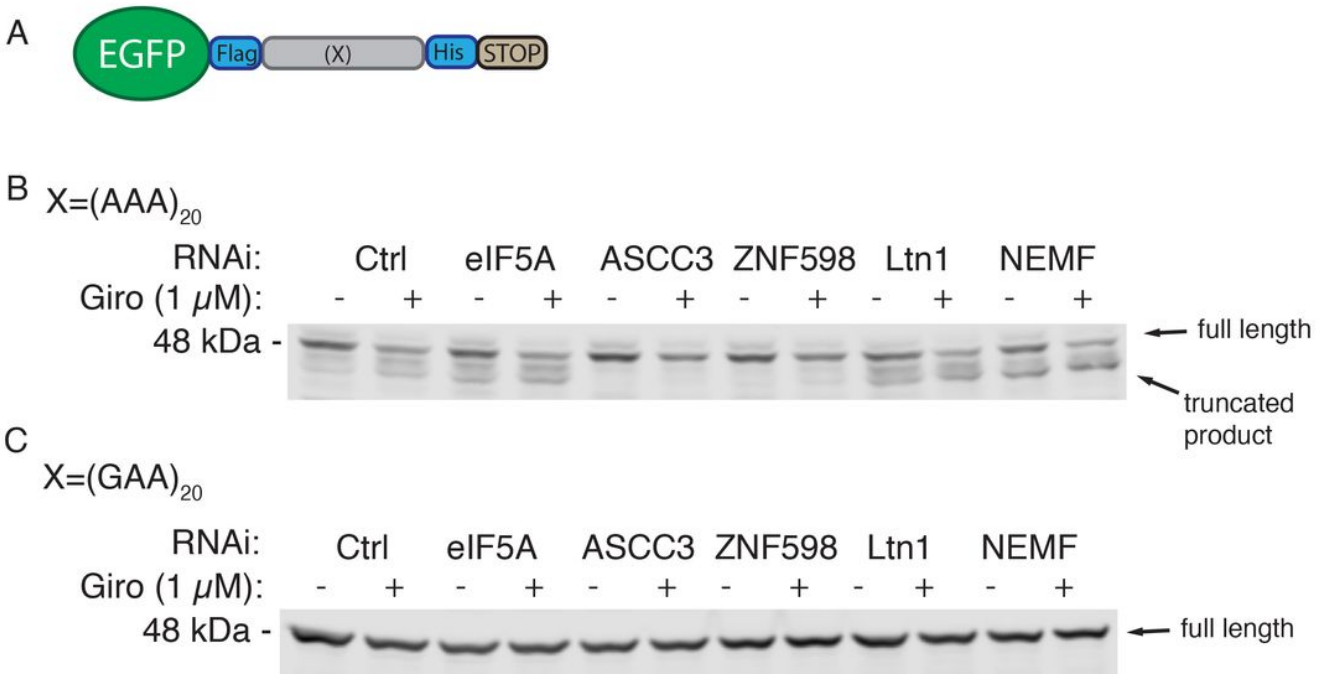

Figure 6

RQC is responsible for premature termination

A. Adjusted reporter construct for immunoblotting. The N-terminal P2A site was deleted and a stop codon was added to the end of the linker. B. Western blot against EGFP for cells depleted in eIF5A and key factors in ribosome quality control, each treated with DMSO control or 1 μM giro. Some stalling was observed in control cells as seen by bands below full length protein but stalling worsened by treatment with giro (arrows). Similar to Fig 5 eIF5A-kd replicates giro-induced phenotype and leads to further stalling. Addition of giro to eIF5A-kd cells increased stalling even more. Depletion of RQC trigger factors ASCC3 and ZNF598 restores translation of reporter to full length and giro loses its effect. Downstream factors Ltn1 and NEMF induce further stalling. C. Neither giro treatment nor depletion of eIF5A or other RQC factors had an effect on translation of a linker containing 20 consecutive GAA codons.

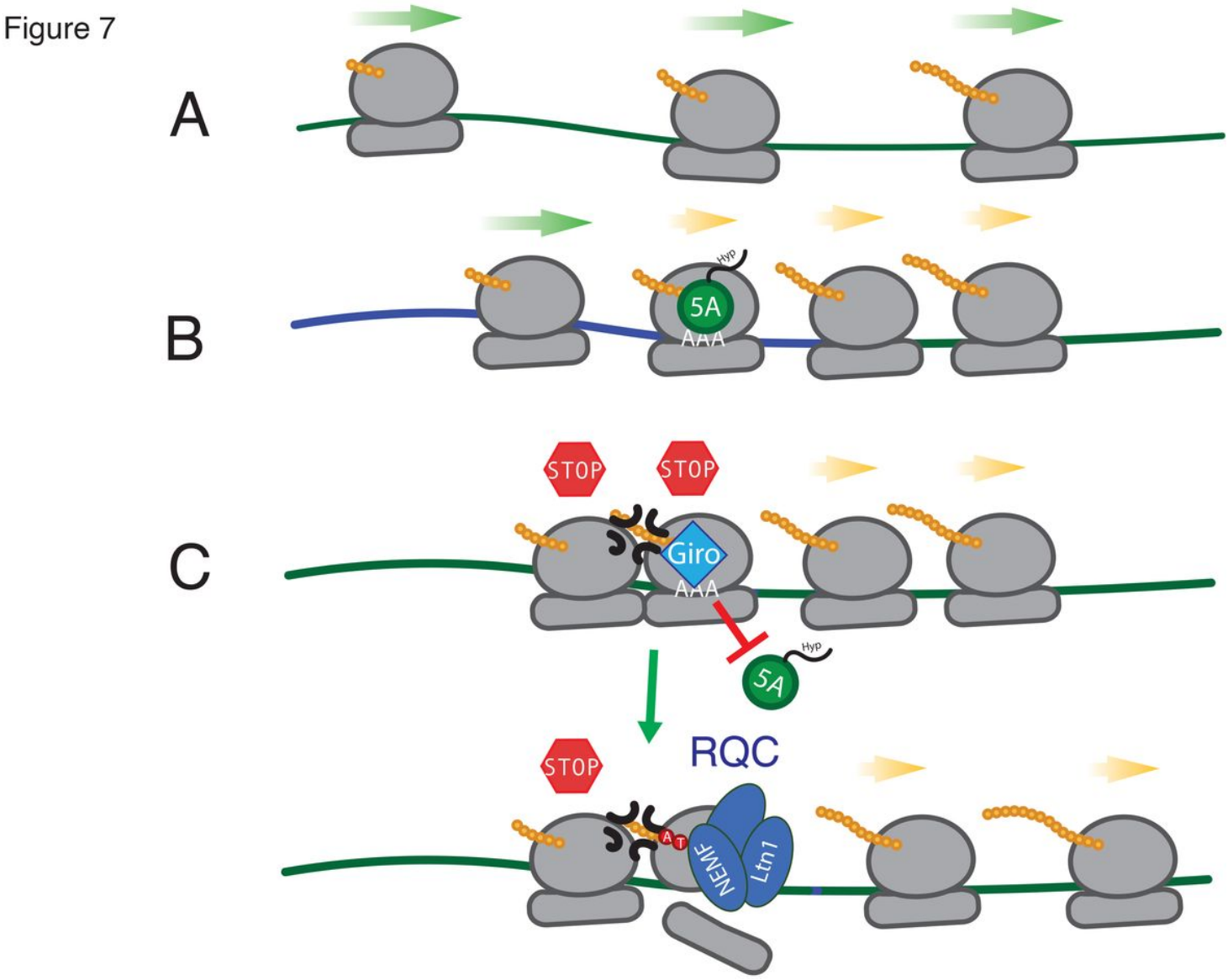

Figure 7

Model

Kinetic model of girolline modulation of eIF5A activity. A. Translation elongation in the absence of challenging sequence stretches does not require eIF5A but B. in presence of difficult to translate sequences eIF5A expedites the elongational progress. C. Giro blocks access of hypusinated eIF5A to the ribosome, causing increased ribosomal stalling and collision, thereby prematurely activating the ribosome quality control pathway (RQC). Green arrows denote fast progress, yellow arrows indicate slowed translation.

Supplementary Files

This is a list of supplementary files associated with this preprint. Click to download.

- SupplementaryTable1.csv
- SupplemtaryVectorMapMap.pdf
- FigureS1.pdf
- FigureS2.pdf
- FigureS3.pdf
- FigureS4.pdf
- FigureS5.pdf
- FigureS6.pdf
- FigureS7.pdf
- FigureS8.pdf